

Quasars as bubbles of dark matter: evidence for axion and tachyon matter in the Universe

Anatoly A. Svidzinsky

Department of Physics, Institute for Quantum Studies, Texas A&M University, TX 77843-4242

(Dated: October 26, 2018)

Growing amount of data show evidence for statistical and apparent physical association between low-redshift galaxies and high-redshift quasi-stellar objects, suggesting noncosmological origin of their redshift and failure of classical quasar explanation. Here we find an analytical solution of Einstein equations describing bubbles made from axions with periodic interaction potential. Such particles are currently considered as one of the leading dark matter candidate. The bubble interior has equal gravitational potential and, hence, photons emitted from the interior possess identical gravitational redshift. The redshift depends on the bubble mass and can have any value between zero and infinity. Quantum pressure supports the bubble against collapse and yields states stable on the scale of the Universe age. Our results explain the observed quantization of quasar redshift and suggest that intrinsically faint point-like quasars associated with nearby galaxies (a few % of known objects) are axionic bubbles with masses 10^8 - $10^9 M_\odot$ and radii 10^3 - $10^4 R_\odot$. They are born in active galaxies and ejected into surrounding space. Properties of such quasars unambiguously indicate presence of axion dark matter in the Universe and yield the axion mass $m = 0.4 - 3$ meV, which fits in the open axion mass window constrained by astrophysical and cosmological arguments.

We also found that tachyons, another dark matter candidate, can form objects with galactic size, negligible mass and any value of the gravitational redshift. Such finding combined with quasar observations suggests that bright quasars 3C 48, 3C 273 and 3C 279 are nuclei of forming nearby small galaxies embedded into tachyonic clots and possess pure gravitational redshift. If the bright quasars later evolve into small companion galaxies, then their dark galactic halos, observed by rotation curves, are probably remnants of the tachyon matter.

I. INTRODUCTION

Since their discovery in 1960's [1] quasars (QSOs) became one of the most mysterious objects in the Universe. All observed QSOs share several remarkable traits. First they are strong sources of radio waves and their radiation spectrum is not a Planck spectrum of thermal radiation as in ordinary stars. Secondly, all QSOs produce radiation with significant redshift, some of them possess redshift $z > 6$. Third, the radiation is characterized by strong emission lines, while ordinary stars produce light with strong absorption lines. Finally, all QSOs have small volumes by galactic standards. One of the most puzzling features is that if the redshift occurs due to large speed of QSOs relative to Earth, they must be cosmological distances away and extremely luminous – their luminosity should lie between 10 and 100 of the total optical luminosity of the brightest galaxies.

The present-day understanding of QSOs is based on the paradigm that redshift of all QSOs has cosmological origin (the so called cosmological hypothesis). Implied huge quasar's luminosity is the main consequence of the cosmological hypothesis. Based on this assumption one can find some similarity between QSOs and active galactic nuclei: both are intense energy producers, both possess strong emission from radio to X-ray bands, sometimes both have jets issuing from the central region. As a result, the present-day conventional view regards QSOs and active galactic nuclei as having the same nature.

The classical (generally accepted) picture of QSOs as active galactic nuclei (AGN) is based on the hypothesis

proposed by Sandage [2] that all QSOs lie in the nuclei of galaxies. The weaker of them are the classical Seyfert 1 nucleus, where the galaxy of stars surrounding the nucleus is clearly seen. In the unified scheme the QSOs are high luminosity Seyfert 1 nuclei which contain a compact nuclear source ionizing a broad line region, surrounded by an optically thick torus of dust. Depending on the orientation of this torus with respect to the line of sight, the central object is seen or hidden. When it is hidden, we see only the narrow, extended emission line region; the galaxy is a Seyfert 2. When it is seen, we see both broad and narrow emission lines. Most radio loud sources have a double lobe structure which is powered by a relativistic jet. When the angle between the jet axis and the line of sight is small the object appears as a blazar.

However, despite of great efforts, the nature of QSOs remains unclear so far. The point is that the unifying scheme in its present form contradicts to some observations which can not be ignored. Problems with the current quasar's paradigm are discussed in many publications and here we mention the main of them (for details see, e.g., [3, 4, 5, 6, 7, 8]). One of the consequences of the unified scheme is that host galaxies of all QSOs must be present. However, observations with Hubble Space Telescope [9, 10] have shown that for some QSOs there are no host galaxies, while for others there is evidence for faint galaxies or irregular systems with the same redshift. Another problem is distances to quasars. Some QSOs and the compact galaxies they evolve into are resolved and many low redshift QSOs lie close to galaxies with approximately the same redshifts [11, 12, 13]. This, as usually believed, suggests on cosmological distances

to the objects. On the other hand, there is a strong evidence that many low redshift (nearby) galaxies and high redshift QSOs are physically associated and, hence, these QSOs are no further away than the close galaxies and must have redshifts noncosmological in origin (see, e.g., [3, 5, 6, 14, 15, 16, 17, 18, 19, 20] and references therein). Observations suggest that such quasars are ejected from active galaxies or in the process of ejection from the galactic nucleus.

A systematic search for quasar-galaxy association was made by Burbidge et al. [14]. They found over 500 close pairs of QSOs and galaxies of which only 28 QSOs were associated with 42 galaxies with approximately equal redshifts (this is what the cosmological hypothesis predicts), while for the reminder 92% objects the quasar redshifts considerably exceeded the galaxy redshifts ($z_{\text{gal}} = 0.0001 - 0.01$). Another evidence is the observation of three QSOs with different large redshifts ($z = 0.60, 1.40, 1.94$) near a spiral arm of the galaxy NGC 1073 by Arp and Sulentic [3]. The galaxy NGC 1073 has much smaller redshift $z = 0.004$ and approximately 16 Mpc away (for $H = 75\text{km/s}\cdot\text{Mpc}$). There are dozens of similar evidences, some of them are discussed in [3, 6, 17, 19, 20, 21, 22]. It is important to note that there is a significant excess of galaxies only around flat spectrum radio-loud QSOs (blazars), which constitute about 10% of the known quasar population. In contrary, there is a marginal defect of galaxies around optically selected QSOs [16, 23].

One of the most fundamental quasar property is the redshift quantization. Based on observations, Karlsson [24] has noted division of quasars into two groups with different redshift properties and concluded the following. If we select QSOs associated with most nearby (distance $d \lesssim 50 - 100$ Mpc), galaxies then their redshift is close to certain values (quantized), as shown in Fig. 4 in next section. Meanwhile, in QSO samples associated with distant, $d \gtrsim 50 - 100$ Mpc, galaxies no periodicity in intrinsic redshift is observed. Such a division is supported by later studies of QSOs associated with most nearby galaxies where the quantization was confirmed [25, 26] and distant ($0.01 < z_{\text{gal}} < 0.3$) galaxies for which absence of any periodicity was claimed [27]. The property suggests existence of intrinsically faint (optical luminosity $L = 10^5 - 10^7 L_{\odot}$) QSO subgroup with quantized noncosmological redshift. Being intrinsically faint, such objects are not detected from large distances which yields disappearance of redshift quantization in distant QSO samples.

The observational evidences indicate that the total quasar population must be divided into several groups having different nature but similar radiation mechanisms. Quasars of the first group are intrinsically faint point-like objects in the optical band and have structure unresolved in telescopes. Such objects are born in nearby active galaxies and ejected into surrounding space. Their redshift is *quantized* and noncosmological (mostly gravitational). Here we show that bubbles of dark matter,

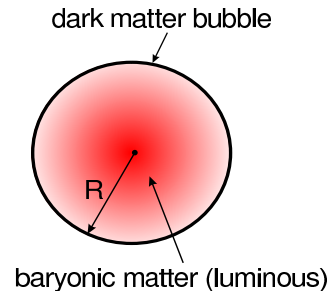


FIG. 1: Structure of intrinsically faint quasars

pictured in Fig. 1, with masses about $10^8 - 10^9 M_{\odot}$ and radii $10^3 - 10^4 R_{\odot}$ can explain the intrinsically faint point-like quasars. The bubble is supported against collapse by quantum pressure and, in principle, can have decay time larger than the age of the Universe. Hypothetical axions, one of the leading dark matter candidate, fit well into this picture and can account for the redshift quantization. Usual baryonic matter falls into the bubble interior, heated by the release of the gravitational energy and produce electromagnetic radiation. The bubble can also harbor a black hole at the center which makes its structure similar to AGN. The amount of baryonic matter trapped in the bubble we assume to be small compared to the bubble mass. Bubble radiation spectrum must be similar to AGN because the radiation mechanism is the same. Photons emitted anywhere inside the bubble interior possess identical gravitational redshift and freely propagate into surrounding space because dark matter is transparent for electromagnetic waves.

Quasars of the second group are intrinsically bright objects with typical optical luminosity $L = 10^8 - 10^{10} L_{\odot}$ (a fraction of the objects can be more luminous). Some of them are resolved in telescopes. Their redshift possesses both the intrinsic and cosmological components, but the intrinsic redshift is *not quantized*. In Section 4 we show that not only small on galactic scale objects can possess large gravitational redshift. Droplets of tachyon dark matter with the mass much smaller than galactic mass can produce any value of the gravitational redshift on kpc scales. Baryonic matter embedded in such regions behaves as being possessed of an intrinsic redshift. Tachyonic clots can explain the nature of intrinsically bright QSOs which possibly have noncosmological redshift component but occupy large space volumes $1 - 100$ pc in size. The classical model of quasars, as active galactic nuclei with pure cosmological redshift, is a limiting case of tachyonic quasars when the gravitational redshift component is negligible compared to the cosmological contribution. Intrinsically bright quasars are observed from substantially greater distances than the faint axionic bubbles and, as a consequence, dominate in the known quasar population. We discuss this issue in the last section.

Luminous active galactic nuclei with pure cosmological

redshift belong to the third group of quasars. However, as we mentioned, there is no sharp distinction between such objects and the tachyonic quasars.

Being intrinsically faint, the axionic bubbles constitute only a few % of the observed QSOs population. Intrinsically bright QSOs are possibly a heterogeneous family. Probably blazars, about 10% of the known QSOs, have the tachyonic nature and their redshift possesses substantial gravitational component. First quasars discovered belong to this category. At the same time, maybe most of the radio-quiet (steep radio spectra) QSOs (about 90% of the known QSOs population) are luminous active galactic nuclei at the cosmological distances indicated by their redshifts. However, the last question requires further analysis.

For the first time our theory was presented at the Fifth International Heidelberg Conference on Dark Matter in Astro and Particle Physics (3-9 October, 2004) [28]; in this paper we provide all the details.

II. DARK MATTER BUBBLES

There is abundant evidence that the mass of the Universe is dominated by dark matter of unknown form [29]. Particle dark matter, i.e., one or more relic particle species from the big bang, is strongly suggested as the dominant component of matter in the Universe [30]. For many years weakly interacting massive particles (WIMPs), such as, for instance, the lightest neutralino in the minimal supersymmetric standard model, were the leading dark matter candidate. However, there is still no evidence in favor of WIMP, either from bolometer experiments designed for direct detection or from the observation of cosmic rays. Moreover, many recent simulations of structure formation in the Universe suggested that any dark matter component modeled as a gas of free particles, such as WIMPs, result in cuspy density profiles at galactic centers, while observation of rotation curves indicate a smooth core density [31]. Such a controversy suggests that the dark matter halo probably consists of a Bose condensate of light particles which behaves as a classical scalar field, coherent on the scale of 10 kpc. Self gravitating Bose condensate, governed by the Klein-Gordon and Einstein equations, could account for the dark matter distribution inside galaxies (see, e.g., [32, 33, 34, 35, 36] and references therein). The field acts as an effective cosmological constant (dark energy) before relaxing into a condensate of nonrelativistic bosons [37, 38]. In order to obtain the Bose condensate halo on the scale of 10 kpc one should consider ultralight noninteracting particles with masses $m \sim 10^{-23}$ eV or heavier particles with self-coupling [32, 39]. From the rotation curve of the Andromeda Galaxy an estimate of the mean mass density of the dark matter composing the 30 kpc luminous core is $\rho \sim 2 \times 10^{-24} \text{kg/m}^3$ [40]. Particle concentration ρ/m determines the temperature of Bose condensation transition T_c . The condition that T_c

is greater than the temperature of the cosmic microwave background radiation imposes an upper limit on the particle mass $m < 1$ eV. So, in order to explain the dark matter halo by a Bose condensate of scalar bosons the particle mass must be in the range $m = 10^{-23} - 1$ eV.

Here we study massive real scalar field φ with periodic interaction potential

$$V(\varphi) = V_0[1 - \cos(\varphi/f)], \quad (1)$$

where $V_0 > 0$. This potential is quite general and derived in quantum field theory in connection with pseudo Nambu-Goldstone bosons (PNGBs) [37, 41, 42]. In all such models, the key ingredients are the scales of global symmetry breaking f and explicit symmetry breaking $(V_0)^{1/4}$. From the viewpoint of quantum field theory, PNGBs are the only way to have naturally ultralow mass, spin 0 particles. One of the example of a light hypothetical PNGB is the axion which possess extraordinarily feeble couplings to matter and radiation and is well-motivated dark matter candidate [30]. Axion arises from the Peccei-Quinn solution to the strong CP problem [43]. If the axion exists, astrophysical and cosmological arguments constrain its mass m to be in the range of $10^{-6} - 3 \times 10^{-3}$ eV and the global symmetry-breaking scale to lie in a narrow window

$$f \approx \frac{m_\pi f_\pi}{2m} = 2 \times 10^9 - 6 \times 10^{12} \text{GeV}, \quad (2)$$

where $m_\pi = 135$ MeV is the neutral pion mass and $f_\pi = 93$ MeV its decay constant [30, 44]. Axions in this mass range could provide much or all of the cold dark matter in the Universe. Interaction of axions with QCD instantons generates the axion mass and cosine interaction potential [45]. Another example of ultralight PNGB is a hypothetical scalar field that arises when the global symmetry is broken on a Planck scale $f \sim 10^{18}$ GeV and explicit breaking scale is comparable to light neutrino mass $(V_0)^{1/4} \sim 10^{-3}$ eV. Such a field, which acquires a mass $m \sim \sqrt{V_0}/f \sim 10^{-24}$ eV, would currently dominate the energy density of the Universe [37].

A self-gravitating real scalar field φ in general relativity is described by the action [46] (in this section we use natural units for which $\hbar = c = 1$)

$$I = \int d^4x \sqrt{-J} \left\{ \frac{1}{16\pi G} R_i - \left[\frac{1}{2} g^{\mu\nu} \partial_\mu \varphi \partial_\nu \varphi + V(\varphi) \right] \right\}, \quad (3)$$

where G is the gravitational constant, J is the determinant of the metric tensor $g_{\mu\nu}$ and R_i is the Riemann curvature. We consider spherically symmetric system, so the metric can be written in the form

$$ds^2 = -N^2 dt^2 + g^2 dr^2 + r^2 d\Omega^2, \quad (4)$$

where g , the radial metric, and N , the lapse, are functions of t and r with r being the circumferential radius. We

introduce dimensionless coordinates and define the unit of distance, time and φ as

$$r_0 = \frac{\hbar}{mc}, \quad t_0 = \frac{\hbar}{mc^2}, \quad \varphi_0 = \frac{1}{\sqrt{4\pi G}}, \quad (5)$$

where c is the speed of light, $m = \sqrt{V_0}/f$ is the mass of the scalar particle. In dimensionless units the coupled Klein-Gordon and Einstein equations describing dynamics of the field φ and the metric are [46]

$$-\frac{\ddot{\varphi}}{N^2} + \frac{\dot{N}\dot{\varphi}}{N^3} + \frac{\varphi'}{g^2} \left(\frac{g^2+1}{r} - 2rg^2V \right) + \frac{\varphi''}{g^2} - \frac{r\dot{\varphi}^2\varphi'}{N^2} - \frac{\partial V}{\partial \varphi} = 0, \quad (6)$$

$$N' = \frac{N}{2} \left[\frac{g^2-1}{r} + r \left(\varphi'^2 - 2g^2V + \frac{g^2\dot{\varphi}^2}{N^2} \right) \right], \quad (7)$$

$$g' = \frac{g}{2} \left[\frac{1-g^2}{r} + r \left(\varphi'^2 + 2g^2V + \frac{g^2\dot{\varphi}^2}{N^2} \right) \right], \quad (8)$$

where an overdot denotes $\partial/\partial t$, a prime denotes $\partial/\partial r$,

$$V = \frac{1}{\alpha^2} [1 - \cos(\alpha\varphi)], \quad \alpha = \frac{1}{\sqrt{4\pi G}f} = \frac{m_{\text{pl}}}{\sqrt{4\pi}f} \quad (9)$$

is the dimensionless potential and the coupling parameter respectively, $m_{\text{pl}} = \sqrt{\hbar c/G} = 1.2 \times 10^{19}$ GeV is the Planck mass. The interaction potential V has degenerate minima at $\varphi = 2\pi n/\alpha$, where n is an integer number. It is tempting to search for time-independent solutions of Eqs. (6)-(8). However, the pseudovirial theorem of Rosen [47] implies that no such solution is possible in the Newtonian limit, and in the strong-field case it has been shown numerically that no nonsingular solution exists [48]. Here we show that in the limit of strong nonlinearity ($\alpha \gg 1$) an approximate time-independent solution does exist and it describes a spherical bubble with surface width much smaller than its radius R . The bubble surface is an interface between two degenerate vacuum states with $\varphi = 2\pi n/\alpha$ ($r < R$) and $\varphi = 0$ ($r > R$).

We look for static solutions, then Eqs. (6)-(8) reduce to

$$\frac{\varphi'}{g^2} \left(\frac{g^2+1}{r} - 2rg^2V \right) + \frac{\varphi''}{g^2} - \frac{\partial V}{\partial \varphi} = 0, \quad (10)$$

$$N' = \frac{N}{2} \left[\frac{g^2-1}{r} + r \left(\varphi'^2 - 2g^2V \right) \right], \quad (11)$$

$$g' = \frac{g}{2} \left[\frac{1-g^2}{r} + r \left(\varphi'^2 + 2g^2V \right) \right], \quad (12)$$

with the following boundary conditions

$$g(0) = g(\infty) = N(\infty) = 1,$$

$$g'(0) = N'(0) = \varphi'(0) = 0, \quad V(\varphi(\infty)) = 0.$$

Outside the bubble $\varphi = 0$ and Eqs. (10)-(12) lead to the Schwazschild solution for a spherically symmetric problem:

$$g^2 = \frac{1}{1-2M/r}, \quad N^2 = 1 - \frac{2M}{r}, \quad (13)$$

where M is the dimensionless bubble's mass in units of m_{pl}^2/m .

Eqs. (10)-(12) can be obtained as an extremum condition of the energy functional

$$E[N, g, \varphi] = \int_0^\infty dr \frac{N}{g} \left\{ r^2 \left(\frac{\varphi'^2}{2} + g^2V \right) - \frac{1}{2}(g-1)^2 + r(g-1) \frac{N'}{N} \right\}. \quad (14)$$

Variation of this functional with respect to φ gives the Klein-Gordon equation (10), while variation with respect to the metric functions g and N yields the Einstein equations (11), (12) respectively. Using Eqs. (12), (14) the total bubble energy reduces to

$$E = \int_0^\infty dr \left[r \left(1 - \frac{1}{g} \right) N \right]' = \lim_{r \rightarrow \infty} r \left(1 - \frac{1}{g} \right) = M, \quad (15)$$

here we applied the Schwazschild solution (13) valid outside the bubble. Eq. (15) demonstrates Einstein equivalence principle between the mass and the energy. Eq. (12) leads also to another expression for the bubble mass:

$$M = \int_0^\infty dr \left[r \left(1 - \frac{1}{g^2} \right) \right]' = \int_0^\infty dr r^2 \left(\frac{\varphi'^2}{g^2} + 2V \right), \quad (16)$$

which shows that the scalar field gradient and the potential V are sources of the bubble energy.

Let us assume that $\alpha \gg 1$ and the radius of the bubble is $R \gg \alpha$. Then inside the bubble, including its surface region, one can omit terms with $1/r$ in Eqs. (10)-(12) and take $r \approx R$ (thickness of the bubble surface is much smaller than its radius), we obtain

$$-2R\varphi'V + \frac{\varphi''}{g^2} - \frac{\partial V}{\partial \varphi} = 0, \quad (17)$$

$$N' = \frac{NR}{2} (\varphi'^2 - 2g^2V), \quad (18)$$

$$g' = \frac{gR}{2} (\varphi'^2 + 2g^2V). \quad (19)$$

Eqs. (17)-(19) can be solved analytically. Their first integral is

$$N = \text{const}, \quad (20)$$

$$\varphi'^2 = 2g^2V, \quad (21)$$

$$g' = Rg\varphi'^2. \quad (22)$$

Further, Eqs. (22) and (21) yield

$$\frac{1}{g} = 1 - R \int_{\varphi}^{\varphi(0)} \sqrt{2V} d\varphi. \quad (23)$$

We assume that $\varphi(0) = 2\pi n/\alpha$, where $n = 1, 2, 3, \dots$ is the number of kinks at the bubble surface, and $\varphi(r)$ monotonically decreases with r . Outside the bubble $\varphi = 0$. Substitute (23) into (21) leads to

$$\varphi' = - \frac{\sqrt{2V}}{1 - R \int_{\varphi}^{\varphi(0)} \sqrt{2V} d\varphi}. \quad (24)$$

Further integration can be made for a particular choice of the scalar field potential. For $V(\varphi)$ given by Eq. (9) the final solution is

$$\begin{aligned} & \frac{4R}{\alpha^2} \ln |\sin(\alpha\varphi/2)| + \left[1 - \frac{4R}{\alpha^2} (2m-1) \right] \text{arctanh}[\cos(\alpha\varphi/2)] \\ & = \text{sign}[\sin(\alpha\varphi/2)](r - R_m), \end{aligned}$$

$$\varphi \in [2\pi(n-m+1)/\alpha, 2\pi(n-m)/\alpha], \quad (25)$$

where R_m is a position of the m th kink, $m = 1, 2, \dots, n$. When the coordinate r passes through the point R_m the scalar field $\varphi(r)$ changes from $2\pi(n-m+1)/\alpha$ to $2\pi(n-m)/\alpha$ (see Fig. 2a). Eq. (23) yields the following expression for g as a function of φ inside the bubble:

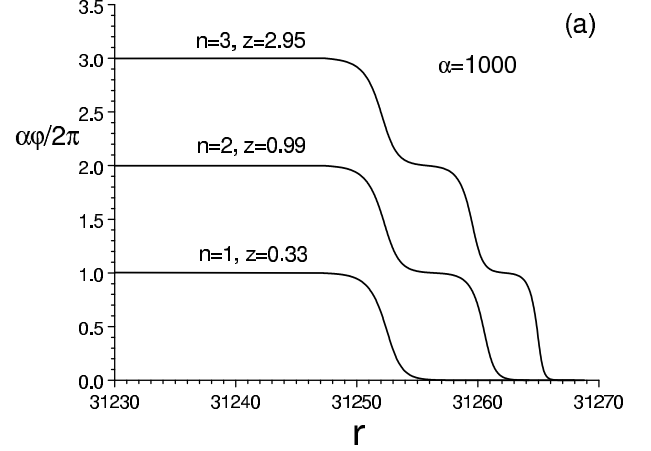
$$\frac{1}{g} = 1 - \frac{4R}{\alpha^2} [2m-1 + \cos(\alpha\varphi/2)]. \quad (26)$$

Outside the bubble $\varphi = 0$, $m = n$ and $1/g = 1 - 8nR/\alpha^2$. The solution is valid if $1/g > 0$, that is $R < R_{\text{max}} = \alpha^2/8n$. Match of the inner solution (26) with the Schwarzschild solution (13) outside the bubble determines the bubble mass:

$$M = \frac{8nR^2}{\alpha^2} - \frac{32n^2R^3}{\alpha^4}. \quad (27)$$

The mass depends on the bubble radius R and changes from zero for $R = 0$ and a maximum value $M_{\text{max}} = \alpha^2/16n$ for $R = R_{\text{max}}$.

The mass-radius relation (27) was derived for the cosine interaction potential (9). However, using Eq. (23),



one can obtain similar relation for any periodic potential $V(\varphi)$

$$M = 4\pi n u R^2 - 8\pi^2 n^2 u^2 R^3, \quad (28)$$

where u is the surface energy density (the energy per unit area) determined by an integral over one potential period

$$u = \frac{1}{4\pi} \int \sqrt{2V} d\varphi. \quad (29)$$

For the cosine potential (9) $u = 2/\pi\alpha^2$.

Redshift of the bubble interior $z = 1/N - 1$ can be found by matching the inner solution $N = \text{const}$ with the Schwarzschild solution (13) outside the bubble. As a result, we obtain that everywhere inside the bubble the redshift is the same and given by

$$z = \frac{1}{\sqrt{1 - 2M/R}} - 1 = \frac{1}{1 - 4\pi n u R} - 1. \quad (30)$$

The internal redshift monotonically increases from zero to infinity when the bubble radius R changes from zero to R_{max} . Fig. 2b shows redshift of space as a function of the distance r to the bubble center. The redshift is constant in the bubble interior and monotonically decreases outside the bubble.

In Fig. 3 we plot the bubble gravitational redshift as a function of its mass for different kink number n . The redshift monotonically increases with the mass and goes to infinity when the mass approaches the maximum value $M_{\text{max}} = \alpha^2/16n$.

A. Redshift quantization

Let us make rescaling $M \rightarrow M/4\pi u$, $R \rightarrow R/4\pi u$, then Eqs. (28), (30) become

$$M = nR^2 - n^2R^3/2, \quad (31)$$

$$z = \frac{1}{1 - nR} - 1. \quad (32)$$

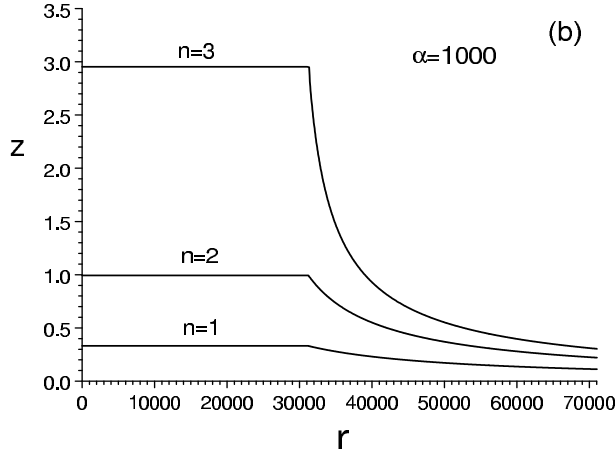


FIG. 2: (a) Scalar field φ as a function of distance r to the bubble center for bubbles with equal radius and different quantum numbers $n = 1, 2, 3$. The unit of length is \hbar/mc . Note, we plot the field φ only in the vicinity of the bubble surface where it undergoes variation. (b) Redshift z of space as a function of distance r to the bubble center for bubbles shown in Fig. 2a. The redshift is constant in the bubble interior.

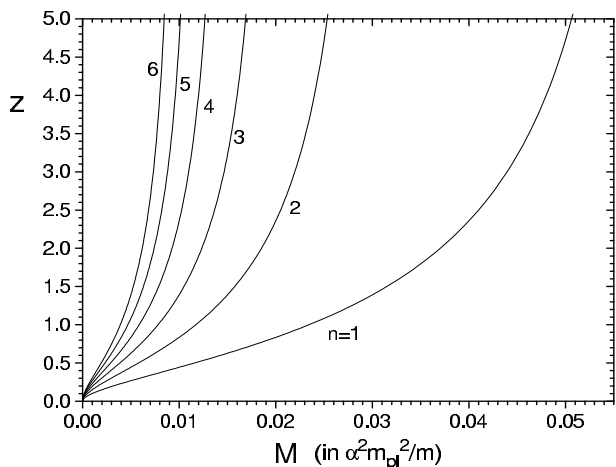


FIG. 3: Redshift of a bubble as a function of mass for different “quantum” numbers $n = 1, 2, 3, 4, 5, 6$.

For a given M the redshift depends on the number of kinks n , which implies that the redshift is quantized.

In early QSO samples involving about 600 radio-emitting QSOs associated with bright nearby spiral galaxies ($z_{\text{gal}} < 0.007$), Karlsson showed that the redshift distribution has a periodicity $\log(1+z_{n+1}) - \log(1+z_n) = 0.089$, where $n = 0, 1, 2, \dots$ and $z_0 = 0.061$ [24, 49]. It has been later confirmed by other groups [25, 50]. In a recent paper, Burbidge and Napier [26] tested for the occurrence of this periodicity in new QSO samples and found it to be present at a high confidence level. The peaks were found at $z \approx 0.30, 0.60, 0.96, 1.41$ and 1.96

n	R , in $\alpha^2 \hbar/mc$	z
1	0.0329	0.357
2	0.0241	0.629
3	0.0204	0.96
4	0.0182	1.40
5	0.0168	2.06
6	0.0159	3.24
7	0.0153	6.11
8	0.0151	26.6

TABLE I: Redshift of the bubble interior z and its radius R for $M = 0.00752\alpha^2 m_{\text{pl}}^2/m$ and different kink numbers n .

in agreement with Karlsson’s empirical formula. The formula also includes the peak at $z_0 = 0.061$, however, this peak does not occur for quasars, but for morphologically related objects.

The redshift periodicity is observed only in QSO samples satisfying certain selection criteria, in particular, the galaxies which are assumed to be paired to the QSOs must be *most nearby* spirals [24, 51]. This implies that redshift quantization is a property of intrinsically faint QSOs which are not detected from large, $\gtrsim 50 - 100$ Mpc, distances. The observed peaks are narrow, implying that the spread in cosmological redshift and Doppler redshift due to random motion must both be small. If they were not, the intrinsic peaks would be washed out, as is easily seen from the combined redshift formula

$$1 + z = (1 + z_g)(1 + z_c)(1 + z_d),$$

where z , z_g , z_c and z_d denote the total, gravitational, cosmological and Doppler redshift respectively. The morphology of companion galaxies is probably also important [51].

If we consider a sample of quasars born in the same type of galaxies it is naturally to expect that such objects would have approximately equal masses because their formation mechanism must be similar. Such phenomenon is well known for type Ia supernovae or neutron stars: practically all measured neutron star masses cluster around the value of $1.4M_\odot$ with only a few percent deviation [52]. If we assume that dark matter bubbles are born with equal masses then their redshift must be quantized. For a given M Eqs. (31), (32) have a set of solutions for R and z corresponding to different values of the “quantum” number n . For $M = 0.0601$ (in dimension units $M = 0.00752\alpha^2 m_{\text{pl}}^2/m$) Eqs. (31), (32) have solutions for $n = 1, 2, \dots, 8$, they are given in Table 1.

In Fig. 4 we plot the most recent histogram of the redshift distribution from Ref. [51] in which five peaks are clearly seen. The solid lines show the redshifts from our Table 1, they match well the observed peaks. The agreement is remarkable because the theory has only one free parameter, the bubble mass M . Such coincidence strongly suggests that some fraction of quasar population is dark matter bubbles composed of scalar particles

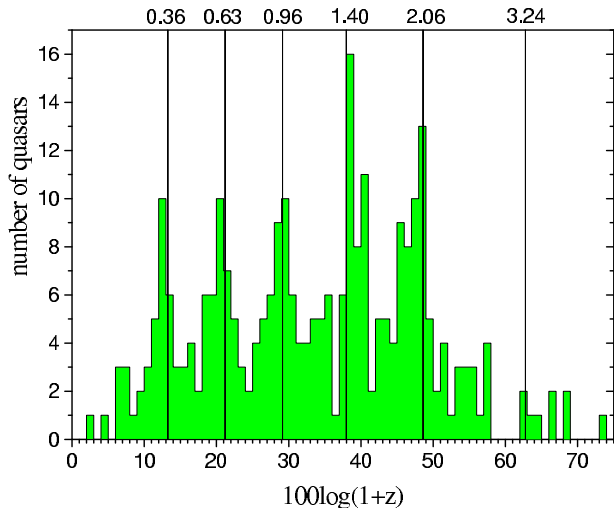


FIG. 4: Histogram of the redshift distribution of QSOs close to bright active spiral galaxies or multiple QSOs with small angular separation from Ref. [51]. The solid lines represent position of the peaks from Table 1.

with periodic interaction potential. One should mention an alternative possibility of quasar evolution. Bubbles can be originally born with the same mass and number of kinks $n = 5$ that corresponds to the 5th peak. During evolution the kinks tunnel to the bubble center and quasars sequentially decay into states with smaller n but the same mass.

If a bubble is made of axions with $m = 10^{-4} - 3 \times 10^{-3}$ eV and $f \approx f_\pi m_\pi / 2m = 2 \times 10^9 - 6 \times 10^{10}$ GeV, then, according to Eq. (9), $\alpha = 5.6 \times 10^7 - 1.7 \times 10^9$. Then a bubble with the internal redshift $z = 0.36$ and $n = 1$ would have the mass $M = 0.00752\alpha^2 m_{\text{pl}}^2 / m = 3 \times 10^7 - 10^9 M_\odot$, surface width $\sim \hbar/mc = 0.07 - 2$ mm, surface mass density $4 \times 10^{12} - 10^{14}$ kg/m² and the radius $R = 0.0329\alpha^2 \hbar/mc = 3 \times 10^2 - 10^4 R_\odot$. Such radius range agrees with the size of the emission region expected for the intrinsically faint point-like quasars associated with nearby galaxies. Indeed, analysis of the emission lines intensity of the bright quasar 3C 48 shows that if it was located a distance of 1000 Mpc then the size of the broad emission-line region should be about 0.1 pc [53]. The quasars we consider as candidates into dark matter bubbles have the apparent visual magnitude 18 - 21 [17, 19] which yields the brightness 1-2 orders smaller than 16th magnitude quasar 3C 48. If they are located 1 - 10 Mpc away and radiating gas has the same parameters as for 3C 48 their size must be of the order of $10^4 R_\odot$ (we assume that the brightness scales as R^3/d^2 , where d is the distance to the object).

An empirical relation between the size of the broad-line region R and luminosity L of Seyfert 1 galaxies, $R \propto L^{1/2}$ [54] yields a similar answer. Indeed, for Seyfert 1 galaxies $R \sim 10 - 100$ light days. The luminosity of the point-like quasars is 5-6 orders smaller, which for the quasars leads

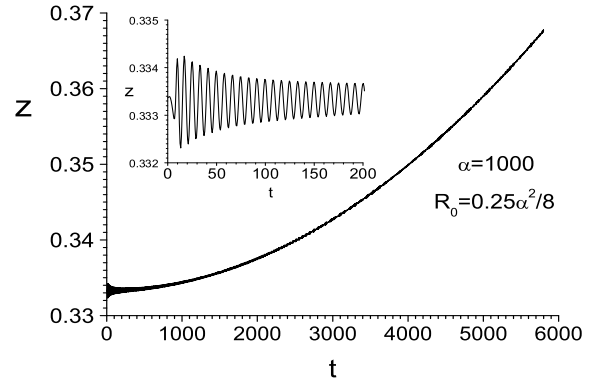


FIG. 5: Redshift of the bubble interior z as a function of time t during collapse of initially static one kink bubble with the radius $R_0 = 0.25\alpha^2/8$ and $\alpha = 1000$. The unit of time is \hbar/mc^2 .

to $R \sim 10^4 R_\odot$.

III. STABILITY

The obtained analytical solution of the stationary equations (10)-(12) is approximate because the terms of the order of $1/\alpha^2$ were omitted. For $\alpha \gg 1$ such terms are very small, however, they play a crucial role in the bubble stability. Our numerical calculations show that the complete system of stationary equations (10)-(12) has no solution which indicates a possible instability. To study the unstable mode we solve numerically the evolution equations for the scalar field (6)-(8) with the initial condition given by the approximate analytical solution (25), (26); the result is shown in Figs. 5 and 6. Under the influence of surface tension and gravitational attraction the initially static bubble starts to collapse very slowly with the acceleration $a = \ddot{R} \sim -c^2/R$ (the corresponding unstable mode has an imaginary frequency $\omega \sim ic/R$). The contraction is accompanied by radiation of scalar particles from the bubble surface which propagate into surrounding space. One can describe the instability as a tendency to reduce the surface area of a hollow bubble with the surface tension $\sigma = u$.

The dynamics of relativistic bubbles has been investigated in connection with the bag model of hadrons and phase transitions in the early Universe [55, 56, 57, 58, 59]. The study has mostly focused on the thin-wall approximation where the bubble surface is specified by effective parameters such as the surface energy density u and the surface tension σ . The approximation omits the particle emission and describes the bubble dynamics by a single differential equation for the radius R . In particular, when $\dot{R} = 0$ the acceleration is given by [56]

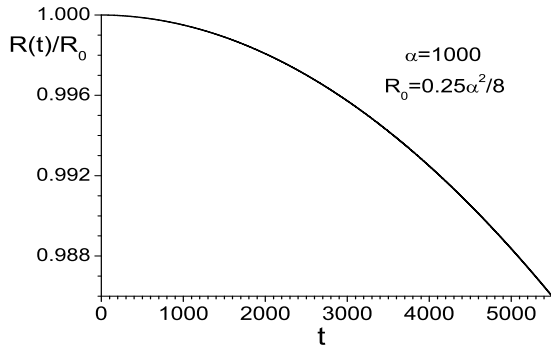


FIG. 6: Radius of the bubble R as a function of time t during collapse of initially static bubble with the radius $R_0 = 0.25\alpha^2/8$ and $\alpha = 1000$. The unit of time is \hbar/mc^2 .

$$u\ddot{R} = -\frac{2N^3\sigma}{R} - \frac{N^2Mu}{(1+N)R^2}, \quad (33)$$

where $N = \sqrt{1 - 2M/R}$. The first term on the right-hand side of Eq. (33) is the Laplace pressure, while the second term is the pressure caused by gravitational attraction. At zero temperature $u = \sigma$. Our numerical result for the surface acceleration (valid at $T = 0$) agrees well quantitatively with Eq. (33) obtained in the thin-wall approximation. This indicates that energy dissipation due to emission of scalar particles is negligibly small and does not affect the bubble contraction.

When the bubble size approaches the gravitational radius $R_g = 2M$ a distant observer sees that shrinking bubble starts to slow down and the shrinking speed decreases to zero. Fig. 7 shows solution of the evolution equations (6)-(8) in the regime when such a behavior is achieved. The bubble radius never crosses the event horizon; in the reference frame of the distant observer the radius $R(t)$ only asymptotically approaches R_g . At large t the bubble radius $R(t)$ is well approximated by an exponentially decaying function shown by dashed line in Fig. 7. The effect is caused by time dilation. Motion of a particle falling into a black hole with a gravitational radius R_g is a classical example of such effect. A distant observer sees that the particle asymptotically approaches R_g , but never crosses it; the particle distance to the center is given by [60]

$$R(t) = R_g + \text{const} \times \exp(-ct/R_g). \quad (34)$$

Radius of the collapsing bubble obeys similar asymptotic behavior; only the coefficient in the exponent differs by a factor of the order of one.

One should mention that if we neglect gravity the bubble would collapse into the origin and disintegrate on a time scale of a few times of the light crossing time R/c

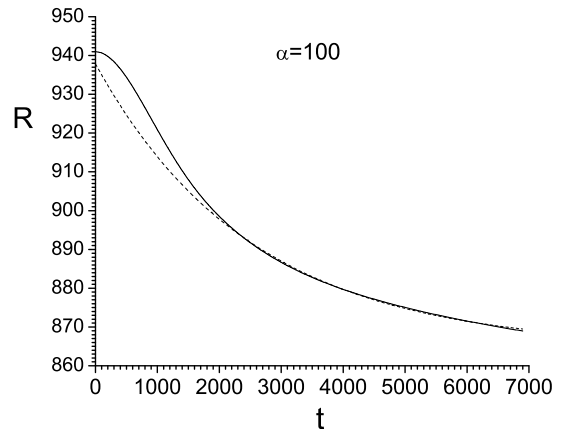


FIG. 7: Radius of the bubble R as a function of time t during collapse of initially static bubble with the radius $R_0 = 941$, initial redshift $z_0 = 3.07$ and $\alpha = 100$ (solid curve). Dashed line shows exponentially decaying fit $R(t) = 865 + 73 \exp(-t/2523)$. The unit of length is \hbar/mc , while the unit of time is \hbar/mc^2 .

[61]. However, if gravity is included this leads to appearance of the event horizon which prevents the bubble collapse into the origin. The bubble life-time in the presence of gravity becomes much larger than R/c . The large value of the bubble life time is a consequence of time dilation produced by gravitation field. In the proper co-ordinate frame the bubble decays on a short time scale $\sim R/c$. However, in the reference frame of a distant observer (which is relevant to quasar problem) the life time is much longer.

For the thin-wall bubble the total mass-radius relation is given by [56, 62]

$$M = \frac{4\pi u R^2}{\sqrt{1 - (dR/d\tau)^2}} - 8\pi^2 u^2 R^3, \quad (35)$$

where τ is the interior coordinate time ($d\tau = Ndt$). When velocity of the bubble surface $dR/d\tau = 0$ the expression (35) reduces to our mass-radius relation (28) for $n = 1$.

A. Quantum stabilization

A classical bubble shrinks towards its gravitation radius R_g and at $t \gg R_g/c$ behaves as a black hole. Such black hole-like objects can not explain the nature of intrinsically faint quasars. Here we show however that quantum effects suppress the collapse and result in appearance of long-lived bubbles (not black holes), stable on the scale of the Universe age. So far we considered the scalar field as classical and Eq. (35) defines the classical equation of motion of the bubble radius. However,

quantum corrections can be crucial for the bubble stability since the later is determined by small terms in Eqs. (10)-(12). It is known that soliton bubbles which are unstable in the classical model can be stabilized by quantum corrections [63, 64]. From the first glance it is somewhat counter-intuitive that for objects $10^4 R_\odot$ in size quantum description is appropriate. However, interaction of dark matter with incoherent environment is extremely weak. Therefore, a coherent state of dark matter can live for a long time, which indicates that the quantum description is probably adequate.

To include quantum effects it has been suggested that the expression (35) for the mass-energy be interpreted as the canonical hamiltonian of the bubble at the quantum level [62, 65, 66]. The bubble wave function $\Psi(R, \tau)$ satisfies the following quantum mechanical equation in 1+1 dimensions ($\hbar = 1$) [62]:

$$\left[\left(-i \frac{\partial}{\partial \tau} + 8\pi^2 u^2 R^3 \right)^2 + \frac{\partial^2}{\partial R^2} - 16\pi^2 u^2 R^4 \right] \Psi(R, \tau) = 0. \quad (36)$$

This equation is interpreted as a one-dimensional wave equation for a relativistic particle moving along the semi-axis $R > 0$ with the boundary condition $\Psi(R = 0) = 0$. Separating variables in Eq. (36) leads to the stationary one-dimensional wave equation [67]

$$\left[(E + 8\pi^2 u^2 R^3)^2 + \frac{\partial^2}{\partial R^2} - 16\pi^2 u^2 R^4 \right] \Psi(R) = 0. \quad (37)$$

This equation possesses stationary solutions that are not possible in the classical model and the energy spectrum of the bubble turns out to be discrete [66, 68]. Such stationary quantum bubbles can explain the nature of intrinsically faint quasars. At the quantum level the collapse is prevented by the uncertainty principle which forbids the exact localization of an extended object in space. The uncertainty principle yields an effective quantum pressure which balances the surface tension and gravitational attraction producing stationary configurations. The discrete energy spectrum can be obtained from the quasi-classical quantization condition

$$\int_0^{R_0} p(R) dR + \pi/4 = (k + 1)\pi, \quad (38)$$

where momentum $p(R)$ is given by

$$p(R) = \sqrt{(E + 8\pi^2 u^2 R^3)^2 - 16\pi^2 u^2 R^4}, \quad (39)$$

$k = 0, 1, 2, \dots$ is the level number and R_0 is the classical turning point at which $p(R) = 0$. The turning point is determined by the classical mass-radius relation (28). In the limit of weak gravity, $uR \ll 1$, Eq. (38) yields the following expression for the energy levels [66]

$$E = 3.59u^{1/3}(k + 3/4)^{2/3}. \quad (40)$$

Bubbles of non-negligible gravitational redshift correspond to highly excited stationary states with $k \gg$

$(\alpha/10)^4 \gg 1$. For such states the spacing between consecutive levels is small compared to the energy and the level distribution can be treated as quasi-continuous.

Let us now estimate the decay rate of the quantum bubble. Partially the picture is analogous to the hydrogen atom where electron moves in the field of nucleus. If initially the electron is localized in a small region at a large distance R from the nucleus then its further motion would be similar to the motion of a classical point particle. The originally resting electron will start to move radially and fall down to the nucleus during the time $t_c \sim \sqrt{R/a}$, where a is the initial acceleration. However, if initially the electron is in a highly excited but stationary state its wave function is delocalized. The uncertainty principle pressure supports such electron cloud from collapse. The decay of the state occurs by means of consecutive transitions between stationary states with smaller principal quantum numbers and energy loss by photon emission. Such decay time t has nothing to do with the time t_c of the classical radial fall of the electron on the nucleus. Nevertheless, t can be estimated from classical equations as the time of energy loss by a point electron performing radial oscillations around the nucleus and emitting electromagnetic waves (even if in the quantum picture there are no such oscillations). Such a rule is a manifestation of the Bohr correspondence principle [69]. This yields $t \sim t_c^4/(R/c)^3 \sim 10^{-8}\text{s}$ which agrees with the quantum mechanical answer for the decay rate of the hydrogen atom excited states, while $t_c \sim 10^{-16}\text{s}$.

The decay of an excited stationary state of the quantum bubble occurs by means of scalar particle emission. We estimate the decay rate using the classical picture as the time of energy loss by the classical bubble with the radius $R(t)$. We are interested in the bubble life-time measured by an outside distant observer. Any correct quantum description cannot avoid the Bohr correspondence principle. So, if the classical bubble treatment, mentioned above, yields very long life-time ($\gg R/c$), the quantum bubble must also be very long-lived.

The outside observer cannot witness crossing of the horizon $R = R_g$ by the bubble surface. As a result, in the reference frame of the distant observer the bubble wave function $\Psi(R, t)$ is equal to zero in the inside region $R < R_g$ [70]. Hence, only the classical trajectory $R(t)$ between the turning point R_0 and the gravitation radius R_g can contribute to the bubble decay rate. Energy loss by the bubble surface becomes substantial only when $R(t) \lesssim R_0^{2/3}$ (see Appendix A below). In our case $R_g \gg R_0^{2/3}$ and, therefore, the region of intensive energy dissipation is not accessible by the classical trajectory. As a result, the energy emission is negligible yielding long-lived stationary states. In Appendix A we estimate the life-time of a quantum bubble as a time of energy loss by the classical bubble with the radius $R(t)$ oscillating between R_0 and R_g ; for an order of magnitude estimate we take the oscillation period to be R_0/c . The answer is

given by Eq. (A11) which in dimension units reads

$$t \sim \frac{z_0^6(z_0 + 2)^6}{(z_0 + 1)^{12}} \frac{R_0}{c} \left(\frac{R_0}{l} \right)^2, \quad (41)$$

where $l = \hbar/mc$ is the surface width and z_0 is the bubble redshift at $R = R_0$. For an axion bubble with $z_0 = 0.3$, $R_0 = 10^2 R_\odot$ and $l < 0.7$ cm Eq. (41) yields $t \gtrsim 10^{18}$ yrs which is much larger than the age of the Universe.

Apart from stabilization, the quantum effects lead to broadening of emission lines. Let us consider an emission line with the wavelength λ_0 produced by atoms inside the bubble. An observer outside the bubble detects the line at the wavelength $\lambda = \lambda_0(1 + z)$, where $z = 1/\sqrt{1 - 2M/R} - 1$ is the redshift of the bubble interior. At a given bubble mass M the redshift depends on the radius R which for the quantum bubble becomes uncertain. Its distribution is determined by the square of the bubble wave function $|\Psi(R)|^2$. Hence, the emission line is detected at the redshift $z(R)$ with a probability proportional to $|\Psi(R)|^2$ and, instead of a sharp line, the observer would detect a broaden peak centered near $z(R)$ corresponding to a maximum of $|\Psi(R)|^2$. In the quasiclassical (WKB) approximation the wave function in the interior coordinate frame can be written as follows [66, 71]

$$\Psi(R) = \frac{C}{\sqrt{p(R)}} \sin \left(\int_R^{R_0} p(x) dx + \frac{\pi}{4} \right) \quad (42)$$

is a solution to the left of the classical turning point R_0 . In the limit of weak gravity ($uR \ll 1$) the normalization constant is $C \simeq 1.24\sqrt{E/R_0}$. In the classical forbidden region $R > R_0$ the wave function decreases as

$$\Psi(R) = \frac{C}{2\sqrt{|p(R)|}} \exp \left(- \int_{R_0}^R |p(x)| dx \right). \quad (43)$$

Near the turning point $p(R) \propto \sqrt{R_0 - R}$. For $R > R_0$, $\Psi(R)$ decays fast on the scale $\Delta R \sim 1/\alpha^{2/3}$, hence, in the classical forbidden region $\Psi(R) \approx 0$. For $R < R_0$, $\Psi(R)$ undergoes fast oscillations. Averaging over the oscillations yields in the vicinity of the turning point

$$|\Psi(R)|^2 \propto \frac{\Theta(R_0 - R)}{\sqrt{R_0 - R}}, \quad (44)$$

where $\Theta(x)$ is the step function. The wave function (44) has a peak at $R = R_0$ and, therefore, the external observer would detect a peak in the bubble radiation spectrum at the wavelength $\lambda' = \lambda_0(1 + z(R_0))$ as if the emission line is redshifted according to the classical mass-radius relation (28). Hence, for the quantum bubbles the same classical Eqs. (28), (30) determine the redshift of the emission features. However, the detected emission line profile $F(\lambda)$ would be different from those emitted by the atom. If for the atom $F(\lambda) \propto \delta(\lambda - \lambda_0)$ then the external observer would detect

$$F(\lambda) \propto \frac{\Theta(\lambda - \lambda')}{\sqrt{\lambda - \lambda'}}. \quad (45)$$

The line profile becomes asymmetric. However, the line width due to quantum broadening is negligible and other broadening mechanisms, e.g., atom motion, would probably wash out the quantum profile.

Finally we emphasize the dramatic difference between the classical and quantum descriptions. In the classical picture the bubble surface localizes after some time at the event horizon which leads to black hole formation. However, due to the uncertainty principle, quantum mechanics does not allow localization of the bubble surface. Eq. (34) suggests that in the reference frame of a distant observer the bubble wave function in the WKB approximation at $R \rightarrow R_g$ behaves as

$$|\Psi(R)|^2 \propto \frac{\Theta(R - R_g)}{R - R_g}. \quad (46)$$

The WKB approximation becomes invalid in a small vicinity of R_g and the exact wave function remains finite. The normalization integral $\int |\Psi(R)|^2 dR$ of the quasiclassical wave function logarithmically diverges at $R \rightarrow R_g$. However, the very slow (logarithmic) divergence suggests that if we cut off the integration at any reasonable distance to R_g the total contribution from the vicinity of R_g is not very large. Hence, in the quantum description there is quite large probability that the bubble radius is substantially greater than R_g . So, in contrast to the classical picture, the long-lived quantum bubble does not behave as a black hole. Light escapes from the bubble interior, but it possesses gravitation redshift determined by Eqs. (28), (30). This is our model of axionic quasars.

One might expect that the $1/(R - R_g)$ divergence of the WKB wave function (46) should produce features in the bubble radiation spectrum at low frequencies. However, the redshift z reduces the radiation power by a factor of $1/(1 + z)^2 = (1 - R_g/R)$ [72]. This compensates the wave function divergence and yields no emission features at low frequencies.

IV. THE NATURE OF BRIGHT QUASARS

The results obtained show that some fraction of quasars is probably bubbles of scalar field with periodic interaction potential. They are born in active galaxies and ejected into surrounding space. The ejection suggests that the bubble mass must be much smaller than the mass of the parent galaxy. A bubble with a mass $10^9 M_\odot$ and gravitational redshift $z = 1$ has a radius $R = 10^{-4}$ pc and, if located at a distance 1 Mpc, would have an angular size of $0.00004''$ which is well below the resolution limit of current telescopes in the optical band ($0.1''$). Therefore, the dark matter bubbles can explain only the faint quasars with unresolved structure. Allowed values of the mass and decay constant f of axion

fit well into this picture suggesting the axion as primary candidate for composition of the dark matter bubbles.

The question whether or not all dark matter in the Universe consists of axions requires further detailed analysis. However, existence of bright quasars with resolved “host” galaxies suggests that some part of dark matter is composed of other particles. Fuzz around bright quasars 3C 48 ($z = 0.37$) [73], 3C 273 ($z = 0.158$) [74], 3C 279 ($z = 0.536$) [75] was found with the redshift equal to the quasar redshift. The angular size of the fuzz is $0.5''$ (3C 279), $4''$ (3C 48) and $10''$ (3C 273). Due to large angular size and brightness such quasars can not be axionic bubbles. However, based on observations, Arp has suggested that 3C 273 and 3C 279 are members of the Virgo cluster (21 Mpc away), while 3C 48 belongs to the Local Group [6]. There is considerable evidence from the morphology [76] and from X-ray emission [77] that this may be the case and, hence, those objects possess noncosmological redshift.

Dark matter bubbles or droplets with radii 10 – 500 pc can explain the observed angular size of the bright quasars provided that the redshift is gravitational. However, if we estimate the required mass from Eq. (30) we obtain $10^{14} - 10^{15} M_\odot$ which is much greater than a typical mass of a large galaxy $10^{12} M_\odot$. Such big masses definitely would not fit into any realistic picture of galaxy clusters and contradict to the scenario of quasar ejection from galaxies.

Here we discuss a solution of the Einstein-Klein-Gordon equations describing an object with galactic size, large gravitational redshift, but possessing negligibly small mass compared to the mass of a galaxy. The solution is similar to a spherical capacitor known in electrostatic. If one plate of the “capacitor” has the mass $+M$, while the other one possesses the mass $-M$ the total mass and gravitational field outside the capacitor is equal to zero. However, the capacitor interior has a nonzero gravitational potential and, hence, nonzero gravitational redshift. Such a capacitor can be realized for scalar fields with negative (attractive) interaction potential. The field kinetic energy provides positive contribution to the energy density, while the contribution from interaction is negative. Space regions where the kinetic energy dominates play a role of the plates with positive mass, while interaction dominating regions are analogous to the negative plates. One can anticipate the effect from the structure of the Einstein equation (11) for the metric component N that determines the space redshift $z = 1/N - 1$. If $V < 0$ then the combination $\varphi'^2 - 2g^2V$ everywhere gives the positive contribution to N producing large total redshift. However, according to Eq. (16), the mass density depends on $\varphi'^2 + 2g^2V$ and if $V < 0$ the total mass can be very small.

To demonstrate the effect we consider a complex scalar field ψ with the simplest attractive potential

$$V(\psi) = -m^2|\psi|^2/2. \quad (47)$$

The free field describes tachyons that always propagate

with the speed greater than the speed of light c , possess momentum $p \geq mc$ and the energy $E = \sqrt{p^2c^2 - m^2c^4}$. There is an evidence that neutrino could be a tachyon [78, 79], which makes the hypothesis that dark matter is partially composed of tachyons not so exotic. Tachyons as a candidate for dark matter and dark energy are currently discussed in the literature (see, e.g., [80, 81, 82] and references therein). They can explain the observations at both large and galactic scales [83, 84].

The equilibrium field configurations are those in which the metric is time independent. The scalar field ψ itself can oscillate with frequency ω , $\psi(t, r) = \psi(r) \exp(-i\omega t)$, however due to U(1) symmetry of the Lagrangian the space-time geometry is static. In dimensionless units, defined by Eq. (5), the stationary Klein-Gordon and Einstein equations for $\psi(r)$ are [46]

$$\frac{\psi'}{g^2} \left(\frac{g^2 + 1}{r} + r g^2 \psi^2 \right) + \frac{\psi''}{g^2} + \frac{\omega^2 \psi}{m^2 N^2} + \psi = 0, \quad (48)$$

$$N' = \frac{N}{2} \left[\frac{g^2 - 1}{r} + r \left(\psi'^2 + g^2 \psi^2 + \frac{\omega^2 g^2 \psi^2}{m^2 N^2} \right) \right], \quad (49)$$

$$g' = \frac{g}{2} \left[\frac{1 - g^2}{r} + r \left(\psi'^2 - g^2 \psi^2 + \frac{\omega^2 g^2 \psi^2}{m^2 N^2} \right) \right]. \quad (50)$$

For simplicity we assume $\omega = 0$. In the limit of zero gravity the Klein-Gordon equation

$$\Delta\psi + \psi = 0 \quad (51)$$

has a spherically symmetric solution

$$\psi = \psi_0 \frac{\sin r}{r} \quad (52)$$

that describes a droplet with specially oscillating energy density $E(r)$ which, at $r \gg 1$, is given by $E(r) = \psi'^2/2 - \psi^2/2 = \psi_0^2 \cos(2r)/2r^2$. The solution is analogous to a set of concentric spherical plates charged alternatively with positive and negative mass.

General relativistic treatment modifies the formula. First we discuss the solution of Eqs. (48)-(50) in the limit $|\psi| \ll 1$. In such limit one can take $g \approx 1$, then Eq. (48) leads to

$$\psi' \left(\frac{2}{r} + r \psi^2 \right) + \psi'' + \psi = 0. \quad (53)$$

Further we take the nonlinear term $r\psi^2$ in the zero order approximation (52). This term is important at $r \gg 1$ and yields a decay of the scalar field faster than $1/r$. Also we average the term $r\psi^2$ over the period of space oscillation, that is assume $r\psi^2 \approx \psi_0^2/2r$, and finally obtain

$$(2 + \psi_0^2/2)\psi'/r + \psi'' + \psi = 0. \quad (54)$$

Solution of this equation is expressed in terms of the Bessel function

$$\psi = \frac{\sqrt{\pi} \psi_0 J_{1/2 + \psi_0^2/4}(r)}{\sqrt{2} r^{1/2 + \psi_0^2/4}} \quad (55)$$

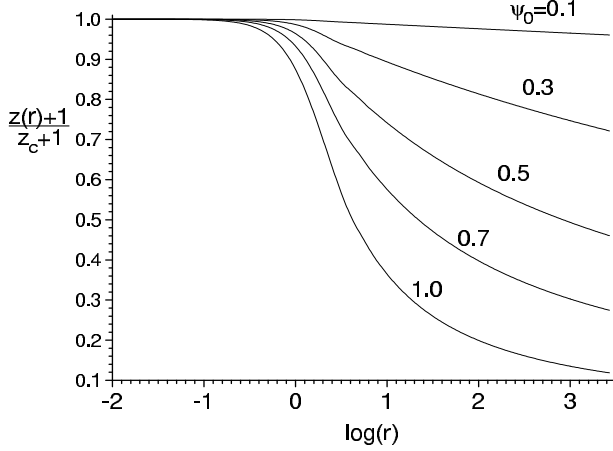


FIG. 8: Redshift $z(r)$ of space as a function of distance r to the droplet center. Note that the redshift is normalized to its center value z_c and the scale along the horizontal axis is logarithmic. The unit of length is \hbar/mc .

and has the following asymptotics: $\psi \approx \psi_0$ at $r \ll 1$, and $\psi \approx \psi_0 \sin r/r^{1+\psi_0^2/4}$ at $r \gg 1$. The total mass-energy of the droplet is (in units m_{pl}^2/m)

$$E = \int_0^\infty r^2 \left(\frac{\psi'^2}{g^2} - \psi^2 \right) dr \lesssim \psi_0^4, \quad (56)$$

which for $\psi_0 \ll 1$ is negligible. However, for the gravitational redshift at the droplet center z_c we obtain

$$z_c \approx \exp \left[\frac{1}{2} \int_0^\infty r(\psi'^2 + \psi^2) dr \right] - 1 = e - 1 = 1.718, \quad (57)$$

the value is independent of ψ_0 (in the limit $\psi_0 \ll 1$). If we move away from the droplet center the redshift of the space decreases from z_c to zero with the asymptotic behavior $z(r) = 1/r^{\psi_0^2/2}$ ($r \gg 1$).

Numerical solution of Eqs. (48)-(50) shows that depending on the scalar field at the droplet center ψ_0 the gravitational redshift can have any large values. In Fig. 8 we plot the spacial distribution of the redshift $z(r)$ for different values of ψ_0 . Near the droplet center the redshift changes on the scale of a few \hbar/mc , while far from the center the spacial variation becomes very weak.

Our model can provide an estimate of the characteristic scales. If, e.g., we take $m = 0.64 \times 10^{-23}$ eV then the unit of length is $\hbar/mc = 1$ pc. A bright baryonic nucleus located a distance $r = 10$ kpc from the center of the tachyonic droplet with $\psi_0 = 0.2$ (the droplet energy $|E| \lesssim \psi_0^4 m_{\text{pl}}^2/m = 10^{10} M_\odot$) would possess a redshift $z = 1/r^{\psi_0^2/2} = 0.83$. Fuzz surrounding the baryonic nucleus with a diameter $\Delta r = 200$ pc would have a dispersion of the gravitational redshift $\Delta z \approx \psi_0^2 \Delta r / 2r^{1+\psi_0^2/2} = 0.00033 = 100$ km/s, the redshift increases towards the droplet center. Such systematic change in the redshift across the fuzz can be directly

measured and serve as a test of our theory. However, the position of the bright nucleus might also coincide with the droplet center, such a picture can be realized provided we choose for m a smaller value.

Our finding shows that substantial gravitational redshift of a large space volume does not necessarily require presence of a big mass. Even a volume of galactic scale can possess any value of the gravitational redshift produced by dark matter with the total mass negligibly small compared to galactic mass. Ordinary baryonic matter placed in such a volume behaves as being possessed of an intrinsic redshift. The effect can explain the nature of intrinsically bright quasars as nuclei of forming nearby small galaxies embedded in a clot of scalar field with negative interaction. It also can account for recent observation of the field surrounding the Seyfert galaxy NGC 7603 where four galaxies with substantially different redshifts are apparently connected by a narrow filament [85].

We want to emphasize that the interaction potential (47) provides a simple demonstration of the effect, rather than a precise quantitative description of the phenomena. Realistic potential must be derived based on detailed study of bright quasars including their environment and, probably, should give rise to a faster asymptotic decay of the scalar field with the distance from the droplet center.

V. DISCUSSION

A. Axions

In this paper we argue that the problems of quasars and dark matter are mutually related. We found that bubbles of scalar field with periodic interaction potential can explain the nature of intrinsically faint point-like quasars associated with nearby galaxies. Typical absolute magnitude M_v of such quasars lies in the range -8 to -13 (optical luminosity $L = 10^5 - 10^7 L_\odot$) [17, 19], the redshift is mostly gravitational and found to be quantized. The bubbles are born in nuclei of active galaxies and ejected into surrounding space. They cluster at a distance upto 100–300 kpc from the parent galaxy. About 15 such objects have been discovered close to M82, the nearest active galaxy to the Milky Way [17], and about 10 in the vicinity of NGC 3628 [22].

The observed five peaks in the quasar redshift distribution match well the theoretical result with only one free parameter, which is a strong argument in favor of our theory. The hypothetical axions, one of the leading dark matter candidate, fit well into the quasar picture and can account for the bubble composition. The axion mass range constrained by astrophysical and cosmological arguments yields the necessary bubble life-time and the size which agrees with the observed quasar brightness.

Properties of the intrinsically faint QSOs, combined with equations for the bubble mass $M = 0.00752\alpha^2 m_{\text{pl}}^2/m = 2.94m(\text{eV}) \times 10^{11} M_\odot$, radius $R =$

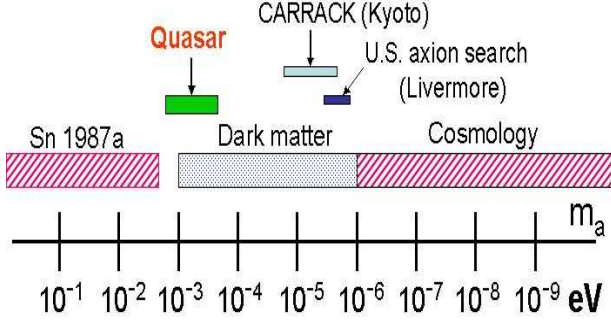


FIG. 9: Astrophysical and cosmological exclusion regions (hatched) for the axion mass m_a . The dotted “inclusion region” indicate where axions could plausibly be the cosmic dark matter. Axion mass determined from quasar observations fits in the open window. Also shown is the projected sensitivity range of the search laboratory experiments for galactic dark matter axions.

$0.0329\alpha^2\hbar/mc = 2.73m(\text{eV}) \times 10^6 R_\odot$ and the relation (2) $m = 0.62 \text{ eV} \times 10^7 \text{ GeV}/f$ [30], allow us to determine the axion mass m . The quasar luminosity suggests that the bubble radius is larger than $10^3 R_\odot$ which yields $m > 4 \times 10^{-4} \text{ eV}$ and $M > 10^8 M_\odot$. From the other hand, the quasar ejection from active galaxies implies that the bubble mass M must be much smaller than the galactic mass. It is reasonable to constrain $M < 10^9 M_\odot$ which leads to $m < 3 \times 10^{-3} \text{ eV}$ and $R < 10^4 R_\odot$. We conclude, the axion mass is $m = 0.4 - 3 \text{ meV}$. This value fits in the open window for the axion mass constrained by astrophysical and cosmological arguments, as displayed in Fig. 9, which unambiguously points towards the axionic nature of dark matter composing the intrinsically faint point-like quasars. One can see that current cavity axion search experiments in Livermore [86, 87] and Kyoto University [30] are looking for the axion in an unlikely mass range which deviates by two orders of magnitude from our result (see Fig. 9). Probably now, when the axion mass is established from quasar observations, the axion has a better chance to be discovered. One should mention that radio telescopes are suited to search for axions of higher mass [88] and allow searches in the range obtained in our paper.

Understanding the mechanisms of quasar formation requires further detailed study. Bose-Einstein condensation of axions in galactic centers can be a possible natural mechanism of bubble creation. Dark matter axions, if they exist, form halos around galaxies. The halo axions are in a quantum degenerate non-equilibrium regime with the de Broglie wavelength $\lambda_d \sim 1 \text{ m}$ which is much larger than the interparticle spacing [30]. The ground state of the system would be a collapsed axion condensate at the galactic center. However, the kinetics of condensate nucleation is governed by two factors: inter-particle collisions and occupation number of the condensate particles. Due to extremely weak interactions between axions the

collision rate is very small, so the galactic halo remains metastable for a long time.

Recent experiments on Bose condensate formation in magnetic traps [89] show that in a weak cooling regime the condensate nucleation occurs in two stages: slow linear growth which then, at a critical point, triggers fast exponentially growing instability, caused by the effect of bosonic stimulation. Similar situation might take place in nuclei of active galaxies. At the first stage, the axions are slowly (during million years) accumulated at the central part of the galaxy. When the mass of such a ball becomes critical (particle occupation number is big enough), it triggers exponential instability due to bosonic stimulation. A dense condensate cloud, coherent on astronomically large scale, starts to form rapidly. The cloud then collapses under its own gravity. Such a mechanism is similar to type Ia supernovae, when a star explodes after accumulation a critical mass, and suggests formation of objects with approximately equal masses. Why does the cloud collapse lead to formation of bubbles? The answer comes from a three-dimensional numerical simulation of the evolution of inhomogeneities in the axion field. Such a simulation has indeed demonstrated formation of bubble-like structures (see Fig. 5a in Ref. [90]). Gravitational cooling is probably an important processes involved in quasar nucleation [91].

Finally we want to mention a new (preliminary) experimental result which became available after our theory was first presented in DARK 2004 [28]. The PVLAS experiment on axion laser production and detection apparently observes a signal which might be produced by axion-like particles [92]. If the observed signal is indeed caused by axions then the particle mass measured in the PVLAS experiment is $m = 1.0 \pm 0.1 \text{ meV}$ [92]. This value is right in the middle of the axion mass interval $0.4 - 3 \text{ meV}$ we predicted based on quasar observations! One should mention that another parameter, the axion-photon coupling, measured by PVLAS is irrelevant to our theory. Our estimate of the axion mass is based only on the relation (2) between the global symmetry-breaking scale f and m . From this perspective one can treat our and PVLAS results as mutually complementary. Only combination of the two independent results confirm, based on observations, the relation (2) which is the key ingredient of any axion model. This provides an evidence that the new particle, detected by PVLAS and responsible for the quasar redshift quantization, is indeed axion and not another yet unknown pseudoscalar particle.

B. Tachyons

Existence of the both intrinsically faint point-like and bright resolved quasars associated with galaxies suggests that dark matter in the Universe is probably composed of several species. We found that tachyonic clots can produce substantial gravitational redshift in a galactic

scale even when the total mass of the object is negligible. Bose condensate of tachyons can explain the nature of intrinsically bright quasars as forming galactic nuclei emerged into droplets of scalar field with negative interaction. The droplets possess large gravitational redshift on kpc scales. About 42 such objects have been discovered in the vicinity of the Seyfert 1 galaxy NGC 6212 which is approximately 120 Mpc away [93]. They form a cloud of QSOs with a characteristic size 2 Mpc and absolute QSO magnitudes from -20 to -15 .

Being large and luminous, the tachyonic objects dominate in samples of quasars associated with relatively distant, $\gtrsim 50$ Mpc, active galaxies. At such distances the axionic bubbles are so faint that they are rarely detectable as individual sources. According to our theory, the redshift quantization is the property of axionic bubbles and must not be present for bright tachyonic quasars. In agreement with the theory, no periodicity in the intrinsic redshift distribution has been found in a sample of tachyon dominating quasars associated with the distant ($0.01 < z_{\text{gal}} < 0.3$) galaxies [27].

If within a distance $d \lesssim 10$ Mpc there are, at least, several bright tachyonic quasars, then inside the region $d \lesssim 100$ Mpc thousands of them must be detected. Probably such objects dominate in the recent First Bright Quasar Survey which radio-selected sources brighter than 18 optical magnitude [94, 95]; axionic bubbles are usually too faint and not selected in such a survey. Luminous tachyonic quasars can be also seen at cosmological distances where the cosmological redshift contribution becomes substantial. The gravitational redshift of tachyonic quasars can also be very small which provides a continuous connection between quasars and active galactic nuclei, the classical quasar explanation. In general case, however, the quasar redshift possesses substantial gravitational component and, hence, is not a measure of the object distance.

Proximity of some quasars and galaxies with approximately equal redshift indicates only that for some objects the gravitational redshift is small compared to cosmological. Meanwhile, the statistical evidence, mentioned in the Introduction, implies that the gravitational redshift dominates for the majority of quasars in the selected sample. It is also worth to note that if a dwarf galaxy lies at a distance of a few kpc from the tachyonic quasar, both such objects are emerged into the same tachyonic clot and, as a consequence, must have close redshifts. This could be a reason why some quasars and associated galaxies possess equal redshifts and account for the nature of binary quasars.

It is known that quasars violate the Hubble redshift-apparent magnitude relation which is an argument against the cosmological redshift. The argument would be very strong if the quasar apparent magnitude m_v proved to be a good indicator of their distance. If objects with equal luminosity possess a uniform space distribution then their number N detected per unit m_v obeys the law $\log(dN/dm_v) = \text{const} + 0.6m_v$ [96]. In Fig. 10 we

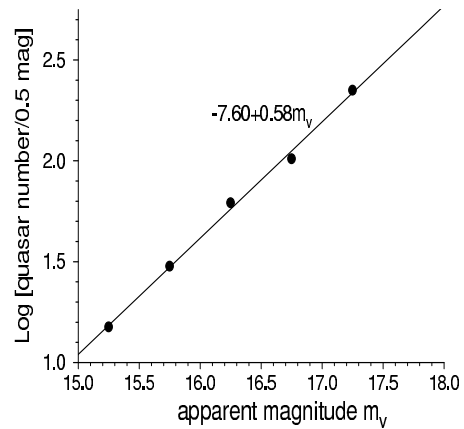


FIG. 10: Logarithm of the number of quasars within the $\Delta m_v = 0.5$ magnitude bins in the First Bright Quasar Survey of the north Galactic cap as a function of the apparent magnitude m_v (dots) [94]. The solid line is the best linear fit.

plot $\log(dN/dm_v)$ as a function of the optical magnitude m_v for quasars discovered by the First Bright Quasar Survey (dots) [94]. The solid line is the best linear fit which yields the slope of 0.58 very close to 0.6. Such an agreement suggests that for a large sample mostly the distance determines m_v of the bright quasars and, hence, the scattered Hubble $z - m_v$ diagram implies noncosmological redshift for the majority of quasars in the Survey.

Arp has noticed an empirical sequence of quasar development in which initially point-like objects at relatively faint apparent magnitudes transform into lower-redshift compact objects with “fuzz” around their perimeters, and then into small, high surface brightness galaxies [6, 97, 98]. In the light of our theory this means that faint axionic bubbles, which are born in and ejected from active galaxies, later serve as nucleation centers for tachyon Bose-Einstein condensation. Condensate formation leads to appearance of a large in size, bright quasar which then gradually transforms into a small companion galaxy. Tachyonic clots can account for the systematic excess of the redshift of small companion galaxies compared to the redshift of the dominant galaxy [6]. Continuity suggests that the dark halos of galaxies, known from their rotation curves, must be remnants of the tachyonic matter. Possibility of such scenario is a subject of future study.

The process of axionic quasar nucleation could produce substantial disturbances in galaxies. Such catastrophic events can contribute to the observed gamma-ray bursts. However, existence of nearby quasars suggests that such events also occur in our epoch, not only in the early Universe. If we divide the total number of galaxies in the Universe, 8×10^{10} , by the frequency of the gamma-ray bursts (~ 1 per day) we obtain that in average the catastrophic event occurs with the interval of 100 million years per galaxy. This value is of the order of the time span between geological periods on Earth which might indicate on their Galactic origin. More often catastrophic events

occurring in the Local galactic group might be responsible for the change in the geological ages within a period. Study of the geological periods on other planets, e.g., on

Mars, can verify this hypothesis.

I wish to thank A. Belyanin and A. Sokolov for helpful discussions.

APPENDIX A: ENERGY EMISSION FROM A SHRINKING BUBBLE

Here we calculate energy loss by a shrinking spherically symmetric bubble caused by emission of scalar particles. For an order of magnitude estimate one can omit the effect of gravity. Then the evolution of the scalar field $\varphi(t, r)$ is described by sine-Gordon equation

$$\ddot{\varphi} - \varphi'' + \sin \varphi = 2\varphi'/r, \quad (\text{A1})$$

where r is the radial coordinate. Without right-hand side, Eq. (A1) has an exact, so-called kink, solution

$$\varphi_0 = 4 \arctan \left\{ \exp \left[\pm \frac{(r - vt - R_0)}{\sqrt{1 - v^2}} \right] \right\}, \quad (\text{A2})$$

where $R_0 \gg 1$ is the initial bubble radius. The solution describes a kink (space region where φ changes from 2π to 0) propagating with constant velocity v ; the kink's size is $l \sim \sqrt{1 - v^2}$.

If $l \ll R(t)$, where $R(t)$ is the bubble radius, r.h.s. of (A1) may be treated as a small perturbation. Eq. (A1) possesses approximate solution in the form of the kink (A2) with parameters slowly changing in time under the action of the perturbation. In particular, the kink shrinks due to its surface tension so that the bubble radius and the velocity evolve as [99]

$$R(t) = R_0 cn(\sqrt{2}t/R_0, 1/\sqrt{2}), \quad v(t) = \sqrt{1 - R^4(t)/R_0^4}, \quad (\text{A3})$$

where cn stands for the elliptic cosine with the modulus $1/\sqrt{2}$. Such a process is accompanied by emission of scalar particles which yields the energy loss. We estimate the energy loss following the original work of Malomed [99, 100]. In terms of the inverse scattering technique, the spectral density of the emitted energy $E_e(t, q)$ is

$$\frac{dE_e}{dq} = \frac{4}{\pi} |B(t, q)|^2, \quad (\text{A4})$$

where q is the radiation wavenumber and the perturbation-induced evolution equation for the complex amplitude $B(t, q)$ is given by [99, 100]

$$\frac{dB}{dt} = -\frac{i}{2(\lambda^2 + \gamma^2)} \int_{-\infty}^{\infty} dr \left(\lambda^2 - \gamma^2 - 2i\lambda\gamma \tanh \left[\frac{r - vt}{\sqrt{1 - v^2}} \right] \right) \exp \left(i\sqrt{1 + q^2}t - iqr \right) \partial_r \varphi_0, \quad (\text{A5})$$

where $\lambda = \sqrt{1 + q^2} - q$ and $\gamma = (1 + v)/2\sqrt{1 - v^2}$. Calculating the integral in (A5) yields

$$\frac{dB}{dt} = \frac{i\pi [\lambda^2(1 - v)(1 - \sqrt{1 + v}) - v/2]}{(1 + v)/4 + \lambda^2(1 - v)} \frac{\exp \left(i\sqrt{1 + q^2}t - iqv t \right)}{\cosh [\pi q \sqrt{1 - v^2}/2]} \quad (\text{A6})$$

If v slowly varies with time one can take $v \approx \text{const}$ in Eq. (A6), then after integration we obtain

$$B(t, q) = \frac{\pi [\lambda^2(1 - v)(1 - \sqrt{1 + v}) - v/2]}{[(1 + v)/4 + \lambda^2(1 - v)] (\sqrt{1 + q^2} - qv)} \frac{\exp \left(i\sqrt{1 + q^2}t - iqv t \right) - 1}{\cosh [\pi q \sqrt{1 - v^2}/2]}. \quad (\text{A7})$$

Therefore

$$\frac{dE_e}{dq} = \frac{16\pi [\lambda^2(1 - v)(1 - \sqrt{1 + v}) - v/2]^2}{[(1 + v)/4 + \lambda^2(1 - v)]^2 (\sqrt{1 + q^2} - qv)^2} \frac{\sin^2 \left[(\sqrt{1 + q^2} - qv) t/2 \right]}{\cosh^2 [\pi q \sqrt{1 - v^2}/2]}. \quad (\text{A8})$$

Integration of (A8) over dq gives the emitted energy as a function of time $E_e(t) = \int_{-\infty}^{\infty} dq(dE_e/dq)$. In Eq. (A8) sine is a fast oscillating function, so we substitute $\sin^2(x) \rightarrow 1/2$. The radiation power increases when the kink's velocity v approaches the speed of light $c = 1$. Assuming $1 - v \ll 1$, integration of Eq. (A8) yields

$$E_e(t) \approx \frac{2.51}{(1 - v(t))^{3/2}} \approx 7.10 \left(\frac{R_0}{R(t)} \right)^6 \quad (\text{A9})$$

The emitted energy becomes comparable with the initial bubble energy $E_0 = 8R_0^2$ when the bubble radius reaches the value $R_* \approx R_0^{2/3}$. This value agrees with those obtained in [61].

If the bubble shrinks from R_0 to the gravitation radius $R_g \gg R_*$ the radiated energy is

$$E_g \sim 7.10 \left(\frac{R_0}{R_g} \right)^6 \approx \frac{(z_0 + 1)^{12}}{z_0^6(z_0 + 2)^6} \frac{E_0}{R_0^2}, \quad (\text{A10})$$

where $z_0 = 1/\sqrt{1 - R_g/R_0} - 1$ is the initial bubble redshift. To emit all its energy the bubble must oscillate between R_g and R_0 about E_0/E_g cycles. As a result, the bubble life-time is

$$t \sim R_0 \frac{E_0}{E_g} \approx \frac{z_0^6(z_0 + 2)^6 R_0^3}{(z_0 + 1)^{12}}, \quad (\text{A11})$$

which for $z_0 = 0.3$ yields $t \sim 0.005 R_0^3$.

-
- | | |
|--|--|
| <p>[1] M. Schmidt, <i>Nature</i> 197, 1040 (1963).
 [2] A.R. Sandage, <i>ApJ</i> 180, 687 (1973).
 [3] H. Arp, <i>Quasars, redshifts and controversies</i>. Interstellar Media, Berkeley, 1987.
 [4] J.V. Narlikar, <i>Space Sci. Rev.</i> 50, 523 (1989).
 [5] G. Burbidge and A. Hewitt, <i>In Variability of blazars</i>, Eds E. Valtaoja and M. Valtonen, Cambridge University Press, Cambridge, p. 4 (1992).
 [6] H. Arp, <i>Seeing red: redshifts, cosmology and academic science</i>. Apeiron, Montreal, 1998.
 [7] A. K. Kembhavi and J. V. Narlikar 1999, <i>Quasars and Active Galactic Nuclei</i>. Cambridge University press, Cambridge, 1999, Sec. 15.
 [8] G. Burbidge, <i>PASP</i>, 113, 899 (2001).
 [9] J. Bahcall, S. Kirkakos, and D. Schneider, <i>ApJ</i> 435, L11 (1994).
 [10] J.B. Hutchings and S. Morris, <i>AJ</i> 109, 1541 (1995).
 [11] A. Stockton, <i>Nature</i> 274, 342 (1978); <i>ApJ</i> 223, 747 (1978).
 [12] T.M. Heckman, G.D. Bothun, B. Balick and E.P. Smith, <i>AJ</i> 89, 958 (1984).
 [13] H.K.C. Yee, <i>AJ</i> 94, 1461 (1987).
 [14] G.R. Burbidge, A. Hewitt, J.V. Narlikar and P. Das Gupta, <i>ApJS</i> 74, 675 (1990).
 [15] G. Burbidge, <i>A&A</i>, 309, 9 (1996).
 [16] N. Benitez and E. Martinez-Gonzalez, <i>ApJ</i> 477, 27 (1997).
 [17] E. M. Burbidge, G. Burbidge, H. Arp and S. Zibetti, <i>ApJ</i> 591, 690 (2003).
 [18] H. Arp, E.M. Burbidge and G. Burbidge, <i>A&A</i> 414, L37 (2004).
 [19] H. Arp, C.M. Gutiérrez and M. López-Corredoira, <i>A&A</i> 418, 877 (2004).
 [20] P. Galianni, E.M. Burbidge, H. Arp, V. Junkkarinen,</p> | <p>G. Burbidge and S. Zibetti, preprint astro-ph/0409215.
 [21] E.M. Burbidge, <i>ApJ</i> 511, L9 (1999).
 [22] H. Arp, E.M. Burbidge, Y. Chu, E. Flesch, F. Patat and G. Rupprecht, <i>A&A</i> 391, 833 (2002).
 [23] I. Ferreras, N. Benitez and E. Martinez-Gonzalez, <i>AJ</i> 114, 1728 (1997).
 [24] K.G. Karlsson, <i>A&A</i> 239, 50 (1990).
 [25] H. Arp, H.G. Bi, Y. Chu and X. Zhu, <i>A&A</i> 239, 33 (1990).
 [26] G. Burbidge and W.M. Napier, <i>AJ</i> 121, 21 (2001).
 [27] E. Hawkins, S.J. Maddox and M.R. Merrifield, <i>MNRAS</i> 336, L13 (2002).
 [28] A.A. Svidzinsky, "Intrinsically faint quasars: evidence for meV axion dark matter in the Universe" in Proceedings of the International Conference DARK 2004, College Station, 3-9 October, 2004, Eds. H.V. Klapdor-Kleingrothaus and R. Arnowitt, Springer (2005); astro-ph/0411548.
 [29] B. Sadoulet, <i>Rev. Mod. Phys.</i> 71, S197 (1999).
 [30] R. Bradley, J. Clarke, D. Kinion, L. J. Rosenberg, K. van Bibber, S. Matsuki, M. Mück and P. Sikivie, <i>Rev. Mod. Phys.</i> 75, 777 (2003).
 [31] B. Moor et al., <i>MNRAS</i> 310, 1147 (1999).
 [32] A. Arbey, J. Lesgourgues and P. Salati, <i>Phys. Rev. D</i> 68, 023511 (2003).
 [33] T. Matos and L.A. Ureña-López, <i>Phys. Rev. D</i> 63, 063506 (2001).
 [34] L.A. Ureña-López and A. R. Liddle, <i>Phys. Rev. D</i> 66, 083005 (2002).
 [35] B. Fuchs and E.W. Mielke, <i>MNRAS</i> 350, 707 (2004).
 [36] T. Matos and G. Torres, <i>RMxAA</i> 39, 113 (2003).
 [37] J.A. Frieman, C.T. Hill, A. Stebbins and I. Waga, <i>Phys. Rev. Lett.</i> 75, 2077 (1995).
 [38] P.T.P. Viana and A.R. Liddle, <i>Astrophysics and Space</i></p> |
|--|--|

- Science **261**, 291 (1999).
- [39] W. Hu, R. Barkana and A. Gruzinov, Phys. Rev. Lett. **85**, 1158 (2000).
 - [40] M.P. Silverman and R.L. Mallett, Class. Quantum Grav. **18**, L103 (2001).
 - [41] C.T. Hill and A.K. Leibovich, Phys. Rev. D **66**, 075010 (2002).
 - [42] C.T. Hill and G.G. Ross, Nuclear Phys. B **311**, 253 (1988).
 - [43] R.D. Peccei and H. Quinn, Phys. Rev. Lett. **38**, 1440 (1977).
 - [44] G. Raffelt, Space Science Rev. **100**, 153 (2002).
 - [45] J.E. Kim, Phys. Rep. **150**, 1 (1987).
 - [46] E. Seidel and W. M. Suen, Phys. Rev. D **42**, 384 (1990).
 - [47] G. Rosen, J. Math. Phys. **7**, 2066 (1966); **7**, 2071 (1966).
 - [48] T. Kodama, K.C. Chung and A.F. da F. Teixeira, Nuovo Cimento **46**, 206 (1978).
 - [49] K.G. Karlsson, A&A **13**, 333 (1971); A&A **58**, 237 (1977).
 - [50] J.M. Barnothy and M.F. Barnothy, PASP **88**, 837 (1976).
 - [51] W.M. Napier and G. Burbidge, MNRAS **342**, 601 (2003).
 - [52] N.K. Glendenning, "Compact Stars: Nuclear Physics, Particle Physics, and General Relativity", Springer Verlag; New York, 2nd edition, (2000).
 - [53] T. X. Thuan, J. B. Oke and J. Bergeron, ApJ **230**, 340 (1979).
 - [54] T.G. Wang and X.G. Zhang, MNRAS **340**, 793 (2003).
 - [55] A. Aurilia, G. Denardo, F. Legovini and E. Spallucci, Phys. Lett. **147B**, 258 (1984).
 - [56] S. K. Blau, E.I. Guendelman and A.H. Guth, Phys. Rev. D **35**, 1747 (1987).
 - [57] A. Aurilia, R.S. Kissack, R. Mann and E. Spallucci, Phys. Rev. D **35**, 2961 (1987).
 - [58] V.A. Berezin, V.A. Kuzmin and I.I. Tkachev, Phys. Rev. D **36**, 2919 (1987).
 - [59] A. Aurilia, M. Palmer and E. Spallucci, Phys. Rev. D **40**, 2511 (1989).
 - [60] See, e.g., L.D. Landau and E.M. Lifshitz "The classical theory of fields", Fizmatlit, Moscow, 7th edition, (1988), Sec. 102.
 - [61] L.M. Widrow, Phys. Rev. D **40**, 1002 (1989).
 - [62] A. Aurilia, R. Balbinot and E. Spallucci, Phys. Lett. B **262**, 222 (1991).
 - [63] V. Baltar, J. Llambías and L. Masperi, Phys. Rev. D **44**, 1214 (1991).
 - [64] M.A. Agüero-Granados, Phys. Lett. A **199**, 185 (1995).
 - [65] V.A. Berezin, N.G. Kozimirov, V.A. Kuzmin and I.I. Tkachev, Phys. Lett. B **212**, 415 (1988).
 - [66] A. Aurilia and E. Spallucci, Phys. Lett. B **251**, 39 (1990).
 - [67] We want to mention that the stationary solution of Eq. (36) is time-independent in the interior coordinate frame; it might be nonstationary in other coordinate systems.
 - [68] P.A. Collins and R.W. Tucker, Nucl. Phys. B **112**, 150 (1976).
 - [69] V.B. Berestetskii, E.M. Lifshitz and L.P. Pitaevskii "Quantum electrodynamics", Fizmatlit, Moscow, 3rd edition, (1989), Sec. 45.
 - [70] Exponentially small penetration of the wave function into the inside region was recently discussed in connection with reflection on event horizon; see, e.g., M.Yu. Kuchiev and V.V. Flambaum, e-print gr-qc/0502117.
 - [71] L.D. Landau and E.M. Lifshits, "Quantum mechanics", Fizmatlit, Moscow, 5th edition, (2001), Sec. 46, 47.
 - [72] C.W. Misner, K.S. Thorne and J.A. Wheeler, "Gravitation", Freeman and Company, New York, (1998), p. 783.
 - [73] G. Canalizo and A. Stockton, ApJ **528**, 201 (2000).
 - [74] H. Hippelein, K. Meisenheimer and H.J. Röser, A&A **316**, 29 (1996).
 - [75] C.C. Cheung, ApJ **581**, L15 (2002).
 - [76] H. Arp and G. Burbidge, ApJL **353**, L1 (1990).
 - [77] H. Arp, Proc. IAU Sym. No 168, Kluwer Academic Publishers, Dordrecht, 1994, p. 401.
 - [78] A. Chodos, A.I. Hauser and A. Kostelecký, Phys. Lett. B **150**, 431 (1985).
 - [79] R.N. Mohapatra, Prog. Partcl. Nucl. Phys. **40**, 55 (1998).
 - [80] G. Shiu and I. Wasserman, Phys. Lett. B **541**, 6 (2002).
 - [81] J.S. Bagla, H.K. Jassal and T. Padmanabhan, Phys. Rev. D **67**, 063504 (2003).
 - [82] P.C.W. Davies, Int. J. Theor. Phys. **43**, 141 (2004).
 - [83] T. Padmanabhan and T. Roy Choudhury, Phys. Rev. D **66**, 081301 (2002).
 - [84] M.B. Causse, astro-ph/0312206.
 - [85] M. López and C.M. Gutiérrez, A&A **421**, 407 (2004).
 - [86] S.J. Asztalos et al., ApJ **571**, L27 (2002).
 - [87] S.J. Asztalos et al., Phys. Rev. D **69**, 011101(R) (2004).
 - [88] B.D. Blout, E.J. Daw, M.P. Decowski, P.T.P. Ho, L.J. Rosenberg and D.B. Yu, ApJ **546**, 825 (2001).
 - [89] M. Köhl, M.J. Davis, C.W. Gardiner, T.W. Hänsch and T. Esslinger, Phys. Rev. Lett. **88**, 080402 (2002).
 - [90] E.W. Kolb and I.I. Tkachev, Phys. Rev. D **49**, 5040 (1994).
 - [91] E. Seidel and W.M. Suen, Phys. Lett. **72**, 2516 (1994).
 - [92] G. Cantatore et al. "First results on dichroism induced by magnetic field in vacuum", talk presented at the National Institute for Nuclear Physics, Trieste, Italy, 4 May, 2005; http://www.ts.infn.it/physics/attivita_scientifica_2005/
 - [93] G. Burbidge, ApJ **586**, L111 (2003).
 - [94] R.L. White et al., ApJS **126**, 133 (2000).
 - [95] R.H. Becker et al., ApJS **135**, 227 (2001).
 - [96] R.M. Soneira and P.J.E. Peebles, ApJ **211**, 1 (1977).
 - [97] H. Arp, J. Astrophys. Astr. **18**, 393 (1997).
 - [98] H. Arp, ApJ **496**, 661 (1998).
 - [99] B.A. Malomed, Physica **24D**, 155 (1987).
 - [100] B.A. Malomed, Phys. Lett. A **123**, 459 (1987).